ACS APPLIED MATERIALS & INTERFACES

Research Article

www.acsami.org

Dimensional Crossover of Thermal Transport in Hybrid Boron Nitride Nanostructures

Navid Sakhavand[†] and Rouzbeh Shahsavari*[,†,‡,§]

[†]Department of Civil and Environmental Engineering, Rice University, Houston, Texas 77005, United States

[‡]Department of Material Science and NanoEngineering, Rice University, Houston, Texas 77005, United States

[§]Smalley Institute for Nanoscale Science and Technology, Rice University, Houston, Texas 77005, United States

Supporting Information

ABSTRACT: Although boron nitride nanotubes (BNNT) and hexagonal-BN (hBN) are superb one-dimensional (1D) and 2D thermal conductors respectively, bringing this quality into 3D remains elusive. Here, we focus on pillared boron nitride (PBN) as a class of 3D BN allotropes and demonstrate how the junctions, pillar length and pillar distance control phonon scattering in PBN and impart tailorable thermal conductivity in 3D. Using reverse nonequilibrium molecular dynamics simulations, our results indicate that although a clear phonon scattering at the junctions accounts for the lower thermal conductivity of PBN compared to its parent BNNT and hBN allotropes, it acts as an effective design tool and provides 3D thermo-mutable features that are absent in the parent structures. Propelled by the junction spacing, while one geometrical parameter, e.g., pillar length, controls the thermal transport along the out-of-plane direction of PBN, the other parameter, e.g., pillar distance, dictates the gross cross-sectional area, which is key for design of 3D thermal management systems. Furthermore, the junctions have a more pronounced effect in creating a Kapitza effect in the out-of-plane direction, due to the change in dimensionality of the phonon transport. This work is the first report on thermo-mutable properties of hybrid BN allotropes and can potentially impact thermal management of other hybrid 3D BN architectures.

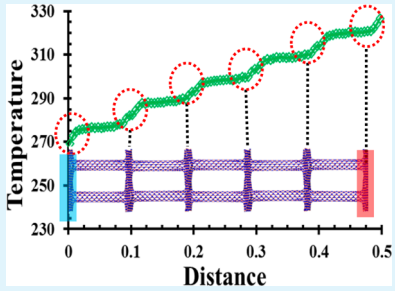

KEYWORDS: *thermal conductivity, anisotropy, phonon scattering, molecular dynamics, Kapitza effect*

INTRODUCTION

Although controlling the heat transport is a well-studied subject in several areas such as thermoelectric materials and energy conservation,[1] with the rapid miniaturization of electronic devices, the heat dissipation is a critical concern.[2] To this end, development of novel low dimensional nanostructures such as nanotubes and nanosheets, which could exhibit super thermal conductivity, is an active area of research for efficient thermal transport applications. In this context, boron nitride allotropes such as boron nitride nanotubes (BNNT)[3] and hexagonal boron nitride sheets (hBN)[2] have attracted increasing interest due to their super thermal conductivity (~350 W/m·K).[3,4] Several other remarkable properties such as thermodynamic (air stable up to 1000 °C)[5−7] and chemical stability,[6] exceptional hardness and corrosion resistivity,[8] and electrically insulating nature[9,10] make them suitable for a wide range of technological and engineering applications. Similar to carbon nanotube (CNT) and graphene, the structures of BNNT and hBN allotropes are made of hexagonal polygons but with alternating boron (B) and nitrogen (N) atoms.[11] Although the mechanical and thermal properties of BNNT and hBN are almost similar to their carbonaceous counterparts, their air stability, super hydrophobicity, piezoelectricity[12] and the electrically insulating nature of the wide bandgap BN clearly differentiate them from CNT and graphene.[13,14]

With all the superb properties of low dimensional materials at the levels of single-wall nanotubes or stacks of sheets a few nanometers in thickness, retaining the efficiency and accuracy of thermal transport properties on a large scale and three-dimensional (3D) scale has remained a challenge. This is mainly due to the high anisotropy of these materials, which leads to directional properties. For example, BNNT and hBN exhibit high thermal conductivity only along the tube axis and in-plane directions, respectively. Large-scale synthesis of these materials or using them as fillers or additives in composites to improve thermal properties result in random orientation of these base materials, thereby decreasing the desired properties by orders of magnitude.[15] This randomness also prevents achieving deterministic thermal conductivity values, which is required for precise design and manufacturing. To address these issues, several efforts have been made to fabricate hybrid nanomaterials with modified or novel properties that are more attractive than their individual parent structures. Examples include carbon nanopeapod,[16] carbon nanobuds,[17] periodic graphene nanobuds,[18] pillared graphene[19] and pillared boron nitride (PBN).[20]

Received: May 7, 2015
Accepted: July 9, 2015
Published: July 9, 2015

DOI: 10.1021/acsami.5b03967
ACS Appl. Mater. Interfaces 2015, 7, 18312−18319

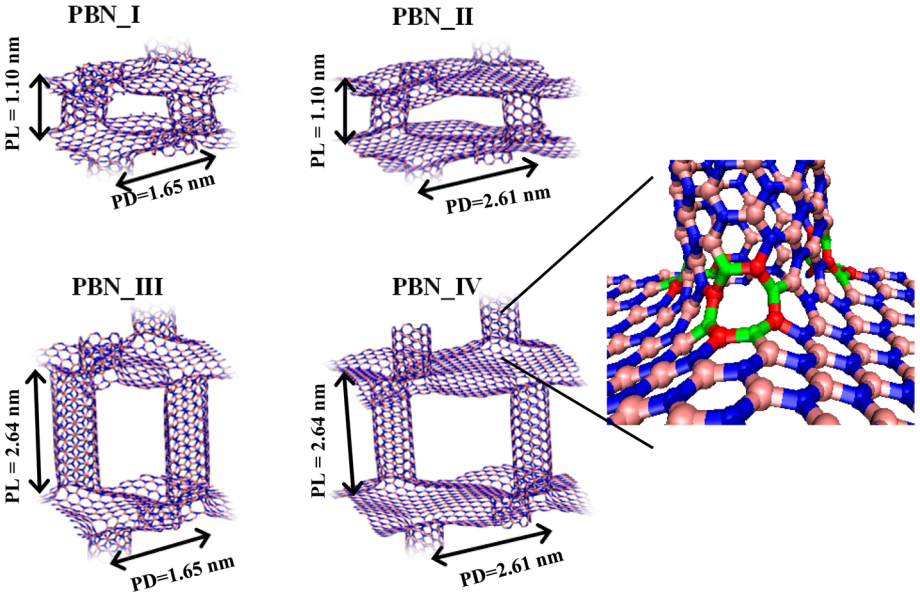

Figure 1. Schematic view of the unit cell of PBN_I to IV prototypes. PBN_I and PBN_III have identical interpillar distances (PDs). PBN_II and PBN_IV have identical pillar lengths (PLs). Schematic of the junction of a pillar and a sheet is shown on the right. The eight-member rings are shown with different colors. Red and pink represent boron atoms; green and blue represent nitrogen atoms.

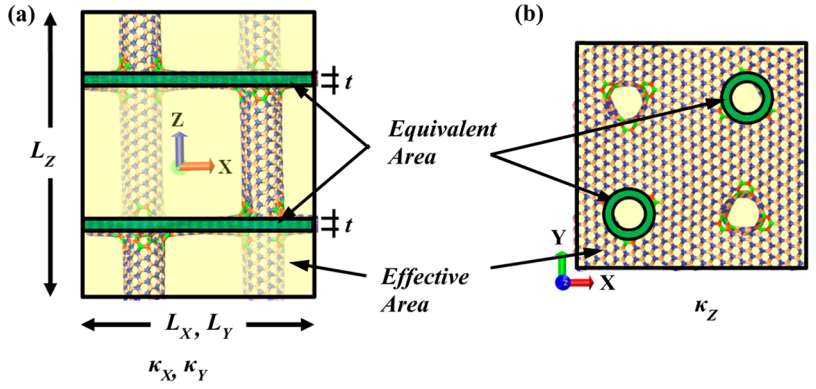

Figure 2. Gross (effective) and equivalent (atomic) areas for (a) *X* and *Y* directions and (b) *Z* direction are shown in yellow and green, respectively. The symbol *t* represents the thickness of the nanotubes and nanosheets and is taken to be 0.33 nm.[47]

Both theoretical and experimental studies indicate that hybrid nanomaterials can leverage the best aspects of their parent structures and/or offer new functionalities depending on the hybrid nanostructure and properties of the constituents.[18,21] Although the majority of the previous reports have been aimed at studying various physio-chemical properties of hybrid carbon-based materials, here we focus on pillared boron nitride (PBN), and use molecular dynamic (MD) simulations to probe its 3D thermo-mutable properties. PBN was recently created as a 3D multifunctional porous BN nanostructure by fusing BNNT as columns and hBN sheets as floors to mediate the high anisotropy associated with its parent constituents and thereby open opportunities for various applications,[20] akin to those offered by its 3D carboneous counterparts. This includes fascinating mechano-mutable functionality with almost 2× increase in out-of-plane ductility and toughness compared to pure BNNT and hBN, ultrahigh surface area and lightweight structure. This makes PBN ideal for gas storage applications because of its 3D articulated structure consisting of a bicontinuous framework as an excellent filler for next generation functional composites, and 3D thermally conductive insulating character, which make PBN a desired choice to complement graphene-based nanoelectronics. Considering heat transport, although both BNNT and hBN are excellent candidates for thermal transport, the molecular junction that covalently connects the BNNT and hBN are prone to phonon scattering, and can serve as thermal hot spots for PBN, thus acting as a bottleneck for many applications and limiting their working efficiency. Therefore, it is imperative to study the influence of junctions on thermal transport properties of PBN and identify important parameters for tailoring associated properties. The focus of the present paper is to study the dimensional crossover of thermal transport, that is, evolution of heat conduction as one goes from 1D and 2D BN allotropes to 3D PBN structures.

RESULTS AND DISCUSSION

Development of Porous Pillared Boron Nitride (PBN) Nanostructure. Among the possible BNNT−hBN junctions, we employed the design of PBN as discussed in an earlier report.[20] In brief, the unit cell of the studied periodic nanostructures was made of four (6,6) BNNTs connected orthogonally to two defected hBN sheets through a negative

DOI: 10.1021/acsami.5b03967
ACS Appl. Mater. Interfaces 2015, 7, 18312−18319

Table 1. Calculated Thermal Conductivities in This Work for Various Sizes of BNNT, hBN and PBN

system	slab direction	length (nm)	equivalent area (nm^2)	thermal conductivity (W/m·K)
		8 layers of hBN		
hBN1	X	5.97	7.38	8.60
hBN2	X	11.93	7.38	22.18
hBN3	X	23.87	7.38	43.72
hBN4	X	47.75	7.38	89.09
hBN5	X	71.61	7.38	126.42
hBN6	X	95.48	7.38	146.25
hBN1	Y	6.15	6.97	8.96
hBN2	Y	12.31	6.97	21.68
hBN3	Y	24.61	6.97	33.89
hBN4	Y	49.22	6.97	88.57
hBN5	Y	73.83	6.97	107.54
hBN6	Y	98.42	6.97	148.04
		(6,6) boron nitride nanotube		
BNNT1	Z	6.33	0.89	13.93
BNNT2	Z	12.15	0.89	21.50
BNNT3	Z	24.30	0.89	40.92
BNNT4	Z	48.84	0.89	61.81
BNNT5	Z	73.10	0.89	76.02
BNNT6	Z	97.66	0.89	85.70
		10 times repeated PBN along slab direction		
PBN_I	X	34.10, 3.46, 2.54[a]	2.35 (8.79)[b]	11.75 (3.15)[c]
PBN_II	X	51.81, 4.99, 2.69	3.39 (13.42)	23.93 (6.05)
PBN_III	X	34.16, 3.46, 6.09	2.35 (21.07)	11.61 (1.3)
PBN_IV	X	51.84, 4.99, 6.28	3.39 (31.34)	25.58 (2.77)
PBN_I	Y	3.40, 34.63, 2.54	2.31 (8.64)	11.40 (3.05)
PBN_II	Y	5.17, 50.03, 2.69	3.52 (13.91)	25.51 (6.45)
PBN_III	Y	3.40, 34.69, 6.09	2.31 (20.71)	11.88 (1.33)
PBN_IV	Y	5.17, 50.00, 6.28	3.52 (32.47)	25.66 (2.78)
PBN_I	Z	3.40, 3.46, 25.38	1.78 (11.76)	5.04 (0.76)
PBN_II	Z	5.17, 4.99, 26.88	1.78 (25.80)	4.69 (0.32)
PBN_III	Z	3.40, 3.46, 61.03	1.78 (11.76)	11.16 (1.68)
PBN_IV	Z	5.17, 4.99, 62.39	1.78 (25.80)	10.59 (0.73)

[a]System dimension in X, Y and Z directions. [b]Effective areas are in parentheses. [c]Thermal conductivity values calculated using the effective area are in parentheses.

Gaussian curvature surface containing 9 hexagonal and 3 octagonal rings, consistent with the generalized Euler's rule of polygons for relating the excess edges (bond surplus) to the topology of the surface. The structural stability of the junction was further confirmed with ab initio calculations. Besides the junction, the pillar length (PL) and interpillar distance (PD) are two other key attributes of PBN that govern many of its hybrid characteristics in 3D.[20] In this study, we considered four PBN prototypes by varying PL and PD as shown in Figure 1. Compared to pillared graphene,[19] these PBN prototypes have wavy sheets, owed to the odd number of nonhexagonal (octagons) rings at the junctions. This imparts an asymmetrical architecture at the junctions, leading to asymmetric strains and wavy hBN sheets (Figure 1).[20]

In-Plane and Out-of-Plane Thermal Conductivities. Table 1 shows the calculated thermal conductivities and system sizes for all four PBN prototypes as well as their parent structures for comparison. All thermal conductivities are calculated using the reverse nonequilibrium molecular dynamics (RNEMD) method.[22,23] For each PBN, thermal conductivity, κ, is independently calculated in X, Y and Z directions at room temperature. The structures were replicated 10 times in the direction of imposed heat flow to minimize the size-effect. In view of the porous structure of PBN, its thermal conductivities are calculated based on realization of two different areas: gross and equivalent (Figure 2). The gross area includes the voids whereas the equivalent area includes only the region where the atoms are present, leading to a smaller total area compared to the gross area. Table 1 shows the thermal conductivities based on both equivalent and gross areas along with slab directions, system sizes and cross-sectional areas. By using equivalent area, thermal conductivity in one direction, e.g., along the tubes PL, becomes less dependent on the size of other direction, i.e., PD. This enables one to compare better the results with pure systems and understand the thermal transport limiting mechanisms, such as effect of BNNT and hBN junctions on phonon scatting in the in-plane or out-of-plane directions. On the contrary, usage of gross area adds further complexity into the system, arising from the changes in the cross-sectional area normal to the heat flow due to consideration of PL or PD. However, gross area is important in system level design,[24] which will be discussed later.

First, we focus on thermal conductivities based on equivalent area. As shown in Figure 3a, the simulated thermal conductivities of pure (6,6) single-wall BNNT and hBN increase with the system size and seem to saturate as the system size becomes too large. This power law behavior is typical in highly thermally conductive materials in which the character-

DOI: 10.1021/acsami.5b03967
ACS Appl. Mater. Interfaces 2015, 7, 18312−18319

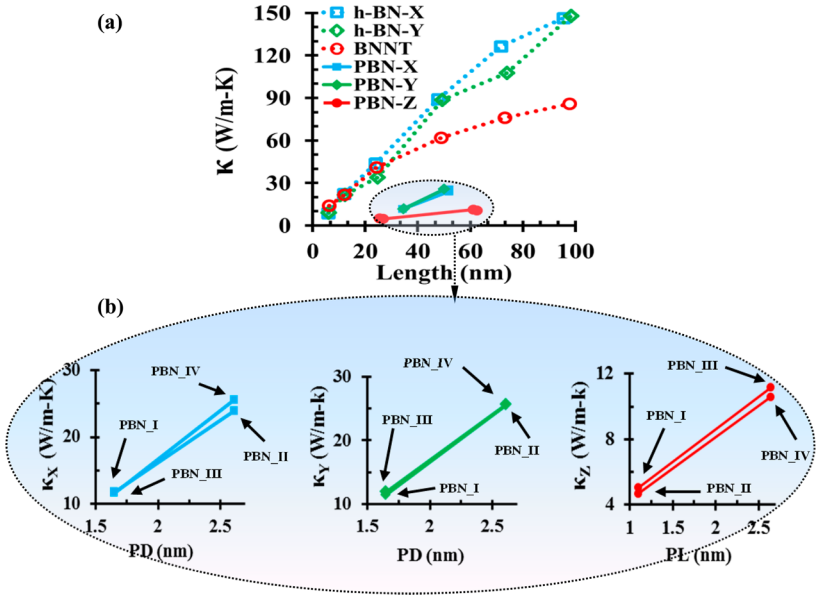

Figure 3. (a) Comparisons of equivalent thermal conductivities of PBN_I to IV prototypes with pure (6,6) BNNT and hBN as a function of size. (b) Zoom-in plots of equivalent thermal conductivities of PBN_I to IV in *X*, *Y* and *Z* directions. For clarity, the abscissas in the inset are represented by PD and PL instead of the overall system size. As a consequence of using the equivalent area, PBNs with identical PDs have almost identical in-plane thermal conductivities. However, along the out-of-plane direction, for an identical PL, there is a weak dependence of κ_z on PD (see text).

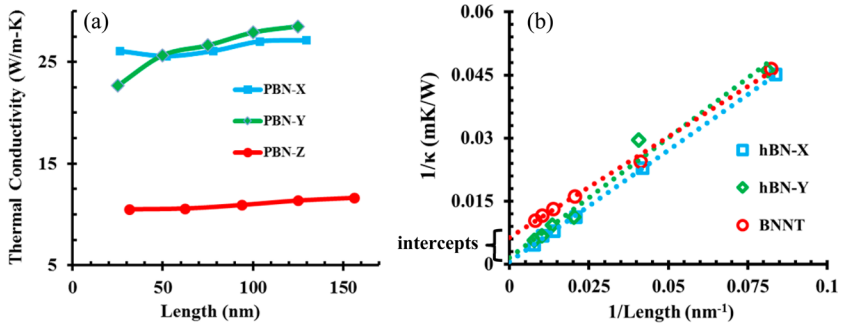

Figure 4. (a) Thermal conductivities of PBN_IV along *X*, *Y* and *Z* directions as a function of the supercell size. (b) Inverse of thermal conductivity and inverse of the length are linearly related. The true values for long lengths are obtained from the intercepts of the fitted lines (dashed lines).

istic mean-free-path is larger than the system size.[15,25−27] Comparison of data for these pure systems with the in-plane and out-of-plane thermal conductivities of PBN in Figure 3a suggests that integration of BNNT in hBN sheets provide scattering points at the junctions, thereby significantly reducing the thermal conductivity of PBN.

The data in Figure 3a depicts that thermal conductivity values in PBN prototypes also increase with the system size. To realize whether it is truly the system size or the PD or PL, which govern the overall thermal conductivity, we conducted a new set of RNEMD simulations on another system. In this case, we focused on PBN_IV and although its PD and PL were fixed, we replicated its unit-cell 5, 10, 15, 20 and 25 times in the *X* direction to calculate thermal conductivity along the *X* axis (κ_X). We repeated a similar procedure for *Y* and *Z* directions as well. The results (Figure 4a) confirm that the thermal conductivities vary minimally with respect to system size. This suggests that it is the PD (PL) that governs the in-plane (out-of-plane) thermal conductivity rather than the absolute system size along the heat flowing direction. This feature can be more clearly observed in Figure 3b where either PD or PL varies. Simply put, when the PD (PL) is large, the scattering of in-plane (out-of-plane) phonons occurs at a longer distance, i.e., junctions. This, in turn, will increase the overall phonon mean-free-path, thus leading to higher thermal conductivity of PBN. In other words, our results indicate that ballistic transport is the major thermal transport mechanism in both the in-plane and out-of-plane directions of PBN. Though this behavior is similar to thermal conductivity variation in pillared graphene,[15,28] we expect that the phonon scattering in PBN is more pronounced than pillared graphene with similar size and dimensions. This is due to (i) different masses of B and N atoms, which result in higher thermal resistance,[24] especially at the junctions, and (ii) the wrinkled configuration of BN sheets, which tend to increase phonon scattering. The latter effect is recently observed in wrinkled (folded) graphene where the in-plane thermal conductivity is lowered by high scattering of low frequency phonons.[29]

Comparison with Parent BNNT and hBN Thermal Conductivities. Another outcome germane to the power law behavior of thermal conductivities of the hBN and BNNT is the prediction of their ultimate thermal conductance. The inverse of thermal conductivity is related to the inverse of the scattering size, l_g (scattering at the heat baths, here the system size) and the mean free path of phonons, l_{ph-ph}, through[30−32]

DOI: 10.1021/acsami.5b03967
ACS Appl. Mater. Interfaces 2015, 7, 18312−18319

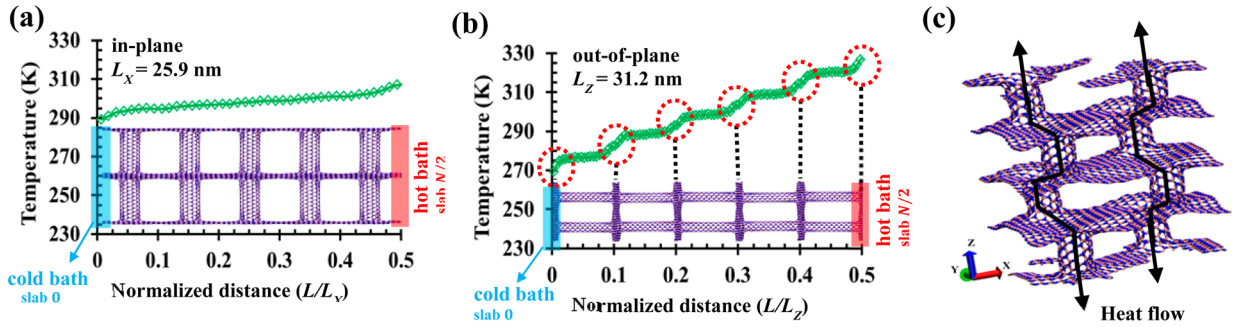

Figure 5. (a) Typical temperature gradient in the in-plane direction, which does not exhibit temperature jumps. (b) Typical temperature gradient in out-of plane direction. The jumps in temperature profile (shown by red circles) are due to discontinuity of the nanotubes. (c) Schematic picture of a stepwise heat flow along the out-of-plane direction. The temperature gradients in panels a and b are shown for a supercell of PBN_IV, replicated 5 times (for better visulization purposes) in the direction where thermal conductivity is calculated. All thermal data reported in this work were derived from 10 times replicated supercells.Because of symmetry, only half of the supercell is shown.

	Kapitza conductance (10^9 W/m^2-K)	
	Effective	Equivalent
PBN_I	0.74	4.93
PBN_II	0.27	3.99
PBN_III	0.61	4.07
PBN_IV	0.27	3.86

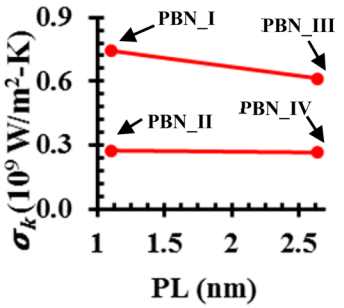

Figure 6. Kapitza conductance for four PBN structures. Either equivalent or effective areas can be used to calculate Kapitza conductance. The figure indicates that the value of Kapitza conductance for PBN structures with similar interpillar lengths are close.

$$\frac{1}{\kappa} \propto \frac{1}{l_g} + \frac{1}{l_{ph-ph}} \quad (1)$$

Because l_{ph-ph} is size independent, by plotting the inverse of thermal conductivity (κ) of hBN and BNNT from Figure 3a and the inverse of the system size, a linear relationship can be observed (see Figure 4b). The intercepts of the fitted lines in Figure 4b correspond to the inverse of asymptotic values of thermal conductivity at very large lengths ($l_g \rightarrow \infty$) where the scattering effect due to system size is eliminated and thermal conductivity values due to phonon scattering are calculated. Via this approach, we calculate the ultimate thermal conductivity of hBN to be ~609 W/m·K. Similarly, we obtain the ultimate thermal conductivity of BNNT to be ~158 W/m·K, lower than hBN, consistent with the previous report.[13,33]

Kapitza Effect in the Out-of-Plane Direction. Within a given PBN, we find that thermal conductivity along out-of-plane direction (κ_Z) is always lower than those along in the in-plane directions, i.e., κ_X and κ_Y (Figure 3a). Although one may expect that this trend stems from intrinsic differences in thermal transport in pure BNNT and hBN, which is also verified by our simulation of pure systems ($\kappa_{BNNT} < \kappa_{hBN}$), there is another crucial factor that comes from the discontinuity of the nanotubes in PBN. For the phonons to be transported from one nanotube to another in the out-of-plane direction, they have to pass through the connecting sheets. These sheets tend to act as a source of interfacial thermal resistance (Kapitza effect) along the out-of-plane direction. This can be clearly observed from the existence of discontinuities in the temperature gradient profiles along the out-of-plane direction (Figure 5b). In fact, the path of phonon transport along the out-of-plane direction involves a stepwise flow going from 1D tubes to 2D sheets to 1D tubes and so on (Figure 5c). This change in dimensionality is expected to contribute to the mismatch in phonon spectra at the junctions, thus further increasing the role of junction scattering as compared to the heat flow along in-plane direction (Figure 5a). The resulting thermal resistance of the PBN prototypes along the out-of-plane direction can be quantified via Kapitza conductance coefficient as[31]

$$\sigma_K = \frac{J}{\Delta T} \quad (2)$$

where J is the heat flux and ΔT is the average temperature jump in the temperature gradient plot of (Figure 5b). Figure 6 shows Kapitza conductance calculated based on both effective and equivalent area. Equivalent Kapitza conductance coefficients are higher than effective ones, as their associated heat flux is higher. From this figure, we also note that Kapitza conductance values are generally similar in magnitudes for PBN structures with similar interpillar distances (PD). However, as PD becomes smaller, the effect of phonon scattering of the junctions per unit area of the sheets is more pronounced, resulting in higher thermal resistance (compare the higher Kapitza conductance of PBN_I versus PBN_II or that of PBN_III versus PBN_V). Analogously, reducing PL typically results in higher Kapitza conductance, owing to the more number of junctions per unit length of the tubes (compare the higher Kapitza conductance of PBN_I versus PBN_III). However, PL seems to be less influential in varying Kapitza conductance compared to the effect of PD (note the almost identical Kapitza conductance of PBN_II versus PBN_V).

In essence, considering both in-plane and out-of-plane equivalent thermal conductivities, the following observation deserves attention: the equivalent thermal transport in the out-

DOI: 10.1021/acsami.5b03967
ACS Appl. Mater. Interfaces 2015, 7, 18312−18319

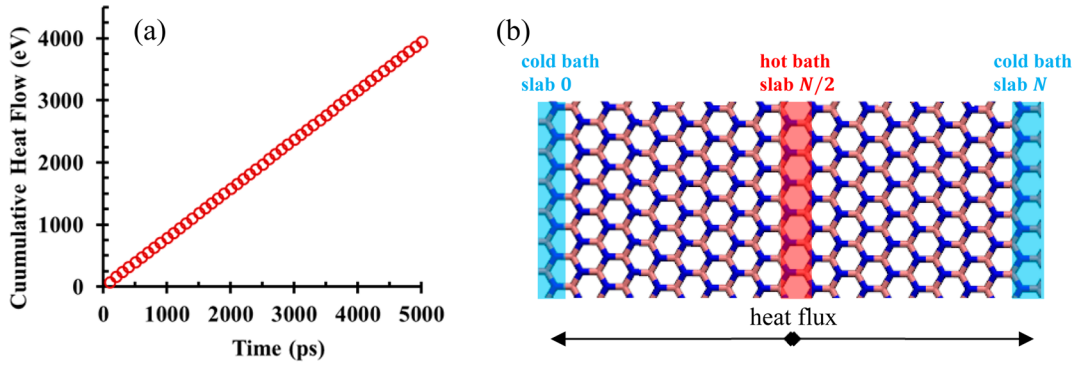

Figure 7. (a) Representative cumulative heat flow for the simulation of PBN_IV in the out-of-plane direction (supercell size 1 × 1 × 5). The heat flux is calculated by dividing the slope of this plot by the area normal to the direction of heat flux. (b) Hot and cold baths in a typical thermal conductivity calculation in aperiodic simulation system. Slabs 0 and N are in contact due to periodicity and have the same temperature.

of-plane direction weakly depends on PD, i.e., the larger the PD, the less likely the effect of change in dimensionality of the heat flow and hence Kapitza effect. However, the equivalent thermal transport along the in-plane direction is independent of the PL. This observation can be verified from the absence of temperature jumps in the junctions associated with the in-plane temperature profile (Figure 5a) as well as the more consistent values of equivalent in-plane thermal conductivities of PBNs with different PL values. For instance, in view of Table 1, the difference between equivalent κ_X in PBN_I with PL = 2.54 nm and PBN_III with PL = 6.09 nm is less than 1.1% (this difference is due to the statistical errors of the numerical algorithm) while the error between equivalent κ_z in PBN_I with PD = 3.40 nm and PBN_II with PD = 5.17 nm is approximately 7%.

Effective Area for Material Design Consideration. Although the use of atomic area enables determining the limiting thermal transport phenomena and phonon scattering mechanisms in PBN, geometric aspects and the overall gross (effective) cross-sectional areas play a crucial role in heat flux from material design perspectives. This is due to spatial inhomogeneity of PBN architectures where both PL and PD affect thermal transport in either direction. As an example, along the in-plane direction, while minimum PD governs the phonon scattering and thus thermal conductance, the PBN prototypes with longer PL (while having identical number of layers) have higher cross-sectional area, hence lower effective in-plane thermal conductivity (see Table 1). Similarly, PD is an important design parameter in determining the effective thermal transport along the nanotube direction. The higher the PD, the lower the effective thermal transport in the out-of-plane direction.[34] In essence, while one distance (e.g., PD) governs the phonon scattering length between the junctions, the other distance (e.g., PL) dictates the overall cross-sectional area and heat flux of the system. This is an important consideration when it comes to designing such 3D template architectures for thermal transport. Thus, in contrast to the equivalent (atomic) thermal conductivity where only out-of-plane thermal transport was weakly dependent on the other direction (i.e., PD), when it comes to actual heat flux and design, both PD and PL must be taken into account simultaneously.

Overall, although the thermal conductivities of PBN prototypes are lower than pure BNNT and hBN, we note that PBN offers 3D thermal transport in both in-plane and out-of-plane directions simultaneously. This feature of PBN (which is absent in pure BNNT and hBN) along with its tunable geometrical parameters (PD and PL) is a key advantage that can be useful for designing tailored thermal transport materials for tuning hybrid composites and layered materials.[35−40]

CONCLUSIONS

In summary, we calculated the thermal conductivities of four PBN prototypes and compared their performance with their parent hBN and BNNT allotropes. With lightweight, porous structure and thermo-mutable anisotropy, PBN provides a multifunctional template for developing 3D nanomaterials with tailored thermal functionality. In this context, the junctions, pillar length (PL) and interpillar distance (PD) emerge as important design parameters that together govern the overall thermal properties of PBN. Of particular importance, the cooperative behavior of the junctions, tubes and sheets in PBN result in unique, inherent 3D characteristics that overcomes the intrinsic limitations of its parent structures, and amplifies its superior properties including 3D balance of thermal transport. Although a clear phonon scattering at the junctions accounts for the lower thermal conductivity of PBN compared to its parent structures, it acts as an effective design tool and provides 3D features that are absent in the parent structures. We demonstrated how tuning PD and PL controls thermal conductivities in the in-plane and out-of-plane directions, respectively. Although the in-plane (out-of-plane) phonon transport and thus thermal conductance of PBN is controlled by PD (PL), the other parameter, PL (PD), determines the gross cross-sectional area, and thus, the total heat flux. The latter is an important factor from material design standpoints for 3D thermal management systems. Furthermore, we found that the junctions have a more pronounced effect in phonon scattering in the out-of-plane direction, leading to an apparent Kapitza effect, due to the discontinuity of the nanotubes and change in dimensionality of the phonon transport. Our results demonstrate potential applications of PBN in heat management devices by simply adjusting the junctions spacing. To the best of our knowledge, this paper, for the first time, probes 3D thermal transport in hybrid BN allotropes and explores their diverse thermo-mutable properties.

EXPERIMENTAL SECTION

Molecular Dynamics Methods. All MD simulations were performed using LAMMPS package[42] with a Tersoff-like potential parametrized for BN interactions,[43] which was previously used for

DOI: 10.1021/acsami.5b03967
ACS Appl. Mater. Interfaces 2015, 7, 18312−18319

BNNT and hBN,[44−47] as well as PBN structures.[20] The four PBN structures were taken from our previous report.[20]

Calculation of Thermal Transport Properties. Before calculation of thermal properties, all the simulations were relaxed for 1 ns. The relaxations were performed under isothermal−isobaric (NPT) ensemble with zero pressure at 298 K, followed by another relaxation under canonical ensemble (NVT). Reverse Noneqauilibrium Molecular Dynamics (RNEMD) method[22,23] was used for calculation of thermal properties where a heat flux is imposed to the system and the resulted temperature gardient is recorded.

To calculate thermal conductance along a particular direction, the unit-cell is replicated 10 times along that direction. A built-in LAMMPS command divides the system into N thin parallel slabs along the desired direction. To impose a heat flux, the velocities of atoms between the adjacent slabs from the cold slab (0) to the hot slab (N/2) are exchanged, while conserving both kinetic energy and momentum. This is important as BN morphologies include two different atoms with different masses (B and N). The transferred heat is calculated as the accumulation of exchanged kinetic energy as

$$Q = \sum_{\text{swaps}} (E_h - E_c) \tag{3}$$

where E_c and E_h are the kinetic energy of the cold and hot slabs, respectively.

The imposed heat flux is a calculated from $J = (Q/2A\Delta t)$, where A is the area normal to the direction of heat flux and Δt is the simulation time (Figure 7a). The division by 2 originates from the heat flowing into two opposite directions from the hot bath (slab N/2 in Figure 7b).

The imposed heat flux results in temperature gradient in the intervening slabs, calculated over time (see Figure 5a,b). The temperature of each slab is then calculated from their kinetic energy as

$$T_i = \frac{1}{3N_i k_B} \sum_{k=1}^{N_i} m_k v_k^2 \tag{4}$$

where N_i is the number of atoms in slab i, m_k, v_k are mass and velocities of atom k, and k_B is Boltzmann constant.

The simulations were performed under microcanonical ensemble (NVE) at 298 K for 5 ns to achieve the steady-state flow where the Fourier's law is valid. At this stage, thermal conductivity, κ, of the system along the imposed gradient direction can be calculated as

$$\kappa = \frac{J}{dT/dz} \tag{5}$$

where dT/dz is the slope of the temperature gradient along the imposed heat flux (J). The temperature gradient and the accumulative heat flow were averaged over time using the following parameters in LAMMPS: input values of every 100 time step (N_{every}); the correlation width (N_{repeat}) of 1000 time step; and the averaged values were recorded every 100 000 time step (N_{freq}). For all the simulations, the swapping of atom velocities was performed every 100 fs.

■ ASSOCIATED CONTENT

Supporting Information

Atomic coordinate of the four PBN prototypes. The Supporting Information is available free of charge on the ACS Publications website at DOI: 10.1021/acsami.5b03967.

■ AUTHOR INFORMATION

Corresponding Author

*R. Shahsavari. E-mail: rouzbeh@rice.edu.

Author Contributions

R.S. designed the research; N.S and R.S performed the computational research and analyzed the data; R.S. wrote the paper.

Notes

The authors declare no competing financial interest.

■ ACKNOWLEDGMENTS

This work was supported in part by the Department of Civil and Environmental Engineering at Rice University and in part by the National Science Foundation grant number CMMI-1235522. The supercomputer machines utilized in this work were supported in part by NIH award NCRR S10RR02950 and an IBM Shared University Research (SUR) Award in partnership with CISCO, Qlogic and Adaptive Computing, and in part by the Data Analysis and Visualization Cyber infrastructure funded by NSF under grant OCI-0959097.

■ REFERENCES

(1) Cahill, D. G.; Braun, P. V.; Chen, G.; Clarke, D. R.; Fan, S.; Goodson, K. E.; Keblinski, P.; King, W. P.; Mahan, G. D.; Majumdar, A.; Maris, H. J.; Phillpot, S. R.; Pop, E.; Shi, L. Nanoscale Thermal Transport. II. 2003−2012. *Appl. Phys. Rev.* **2014**, *1*, 1−45.

(2) Zhou, H.; Zhu, J.; Liu, Z.; Yan, Z.; Fan, X.; Lin, J.; Wang, G.; Yan, Q.; Yu, T.; Ajayan, P.; Tour, J. High Thermal Conductivity of Suspended Few-Layer Hexagonal Boron Nitride Sheets. *Nano Res.* **2014**, *7*, 1232−1240.

(3) Chang, C. W.; Fennimore, A. M.; Afanasiev, A.; Okawa, D.; Ikuno, T.; Garcia, H.; Li, D.; Majumdar, A.; Zettl, A. Isotope Effect on the Thermal Conductivity of Boron Nitride Nanotubes. *Phys. Rev. Lett.* **2006**, *97*, 085901.

(4) Hu, J.; Ruan, X.; Chen, Y. P. Thermal Conductivity and Thermal Rectification in Graphene Nanoribbons: A Molecular Dynamics Study. *Nano Lett.* **2009**, *9*, 2730−2735.

(5) Chen, Y.; Zou, J.; Campbell, S. J.; Caer, G. L. Boron Nitride Nanotubes: Pronounced Resistance to Oxidation. *Appl. Phys. Lett.* **2004**, *84*, 2430−2432.

(6) Golberg, D.; Bando, Y.; Kurashima, K.; Sato, T. Synthesis and Characterization of Ropes Made of BN Multiwalled Nanotubes. *Scr. Mater.* **2001**, *44*, 1561−1565.

(7) Golberg, D.; Bando, Y.; Tang, C. C.; Zhi, C. Y. Boron Nitride Nanotubes. *Adv. Mater.* **2007**, *19*, 2413−2432.

(8) Miyoshi, K.; Buckley, D. H.; Pouch, J. J.; Alterovitz, S. A.; Sliney, H. E. Mechanical Strength and Tribological Behavior of Ion-Beam-Deposited Boron Nitride Films on Non-Metallic Substrates. *Surf. Coat. Technol.* **1987**, *33*, 221−233.

(9) Blase, X.; Rubio, A.; Louie, S. G.; Cohen, M. L. Stability and Band Gap Constancy of Boron Nitride Nanotubes. *Europhys. Lett.* **1994**, *28*, 335−340.

(10) Rubio, A.; Corkill, J. L.; Cohen, M. Theory of Graphitic Boron Nitride Nanotubes. *Phys. Rev. B: Condens. Matter Mater. Phys.* **1994**, *49*, 5081−5084.

(11) Gannett, W.; Regan, W.; Watanabe, K.; Taniguchi, T.; Crommie, M. F.; Zettl, A. Boron Nitride Substrates for High Mobility Chemical Vapor Deposited Graphene. *Appl. Phys. Lett.* **2011**, *98*, 242105.

(12) Nakhmanson, S. M.; Calzolari, A.; Meunier, V.; Bernholc, J.; Nardelli, M. B. Spontaneous Polarization and Piezoelectricity in Boron Nitride Nanotubes. *Phys. Rev. B: Condens. Matter Mater. Phys.* **2003**, *67*, 235406.

(13) Golberg, D.; Bando, Y.; Huang, Y.; Terao, T.; Mitome, M.; Tang, C.; Zhi, C. Boron Nitride Nanotubes and Nanosheets. *ACS Nano* **2010**, *4*, 2979−2993.

(14) Li, X.; Zhang, G.; Bai, X.; Sun, X.; Wang, X.; Wang, E.; Dai, H. Highly conducting graphene sheets and Langmuir-Blodgett films. *Nat. Nanotechnol.* **2008**, *3*, 538−542.

(15) Varshney, V.; Patnaik, S. S.; Roy, A. K.; Froudakis, G.; Farmer, B. L. Modeling of Thermal Transport in Pillared-Graphene Architectures. *ACS Nano* **2010**, *4*, 1153−1161.

(16) Lee, J.; Kim, H.; Kahng, S. J.; Kim, G.; Son, Y. W.; Ihm, J.; Kato, H.; Wang, Z. W.; Okazaki, T.; Shinohara, H.; Kuk, Y. Bandgap

DOI: 10.1021/acsami.5b03967
ACS Appl. Mater. Interfaces 2015, 7, 18312−18319

Modulation of Carbon Nanotubes by Encapsulated Metallofullerenes. *Nature* **2002**, *415*, 1005−1008.
(17) Nasibulin, A. G.; Pikhitsa, P. V.; Jiang, H.; Brown, D. P.; Krasheninnikov, A. V.; Anisimov, A. S.; Queipo, P.; Moisala, A.; Gonzalez, D.; Lientschnig, G.; Hassanien, A.; Shandakov, S. D.; Lolli, G.; Resasco, D. E.; Choi, M.; Tomanek, D.; Kauppinen, E. I. A Novel Hybrid Carbon Material. *Nat. Nanotechnol.* **2007**, *2*, 156−161.
(18) Wu, X.; Zeng, X. C. Periodic Graphene Nanobuds. *Nano Lett.* **2009**, *9*, 250−256.
(19) Dimitrakakis, G. K.; Tylianakis, E.; Froudakis, G. E. Pillared Graphene: A New 3-D Network Nanostructure for Enhanced Hydrogen Storage. *Nano Lett.* **2008**, *8*, 3166−3170.
(20) Sakhavand, N.; Shahsavari, R. Synergistic Behavior of Tubes, Junctions, and Sheets Imparts Mechano-Mutable Functionality in 3D Porous Boron Nitride Nanostructures. *J. Phys. Chem. C* **2014**, *118*, 22730−22738.
(21) Song, L.; Liu, Z.; Reddy, A. L. M.; Narayanan, N. T.; Taha-Tijerina, J.; Peng, J.; Gao, G.; Lou, J.; Vajtai, R.; Ajayan, P. M. Binary and Ternary Atomic Layers Built from Carbon, Boron, and Nitrogen. *Adv. Mater.* **2012**, *24*, 4878−4895.
(22) Müller-Plathe, F. A Simple Nonequilibrium Molecular Dynamics Method for Calculating the Thermal Conductivity. *J. Chem. Phys.* **1997**, *106*, 6082−6085.
(23) Müller-Plathe, F. Reversing the Perturbation in Nonequilibrium Molecular Dynamics: An Easy Way to Calculate the Shear Viscosity of Fluids. *Phys. Rev. E: Stat. Phys., Plasmas, Fluids, Relat. Interdiscip. Top.* **1999**, *59*, 4894−4898.
(24) Varshney, V.; Roy, A. K.; Froudakis, G.; Farmer, B. L. Molecular Dynamics Simulations of Thermal Transport in Porous Nanotube Network Structures. *Nanoscale* **2011**, *3*, 3679−84.
(25) Che, J.; Çagin, T.; Goddard, W. A., III Thermal conductivity of carbon nanotubes. *Nanotechnology* **2000**, *11*, 65.
(26) Maruyama, S. A Molecular Dynamics Simulation of Heat Conduction in Finite Length Swnts. *Phys. B* **2002**, *323*, 193−195.
(27) Mingo, N.; Broido, D. A. Length Dependence of Carbon Nanotube Thermal Conductivity and the "Problem of Long Waves. *Nano Lett.* **2005**, *5*, 1221−1225.
(28) Park, J.; Prakash, V. Thermal Transport in 3D Pillared SWCNT−Graphene Nanostructures. *J. Mater. Res.* **2013**, *28*, 940−951.
(29) Yang, N.; Ni, X.; Jiang, J.-W.; Li, B. How Does Folding Modulate Thermal Conductivity of Graphene? *Appl. Phys. Lett.* **2012**, *100*, 093107−4.
(30) Bagri, A.; Kim, S.-P.; Ruoff, R. S.; Shenoy, V. B. Thermal transport across Twin Grain Boundaries in Polycrystalline Graphene from Nonequilibrium Molecular Dynamics Simulations. *Nano Lett.* **2011**, *11*, 3917−3921.
(31) Schelling, P. K.; Phillpot, S. R.; Keblinski, P. Comparison of atomic-level simulation methods for computing thermal conductivity. *Phys. Rev. B: Condens. Matter Mater. Phys.* **2002**, *65*, 144306.
(32) Sellan, D. P.; Landry, E. S.; Turney, J. E.; McGaughey, A. J. H.; Amon, C. H. Size effects in molecular dynamics thermal conductivity predictions. *Phys. Rev. B: Condens. Matter Mater. Phys.* **2010**, *81*, 214305.
(33) Jo, I.; Pettes, M. T.; Kim, J.; Watanabe, K.; Taniguchi, T.; Yao, Z.; Shi, L. Thermal Conductivity and Phonon Transport in Suspended Few-Layer Hexagonal Boron Nitride. *Nano Lett.* **2013**, *13*, 550−554.
(34) Yu, M.-F.; Lourie, O.; Dyer, M. J.; Moloni, K.; Kelly, T. F.; Ruoff, R. S. Strength and Breaking Mechanism of Multiwalled Carbon Nanotubes Under Tensile Load. *Science* **2000**, *287*, 637−640.
(35) Rafiee, M. A.; Narayanan, T. N.; Hashim, D. P.; Sakhavand, N.; Shahsavari, R.; Vajtai, R.; Ajayan, P. M. Hexagonal Boron Nitride and Graphite Oxide Reinforced Multifunctional Porous Cement Composites. *Adv. Funct. Mater.* **2013**, *23*, 5624−5630.
(36) Sakhavand, N.; Shahsavari, R. Universal Composition-Structure-Property Maps for Natural and Biomimetic Platelet-Matrix Composites and Stacked Heterostructures. *Nat. Commun.* **2015**, *6*, 6523.
(37) Sakhavand, N.; Muthuramalingam, P.; Shahsavari, R. Toughness Governs the Rupture of the Interfacial H-Bond Assemblies at a Critical Length Scale in Hybrid Materials. *Langmuir* **2013**, *29*, 8154−8163.
(38) Jalilvand, S.; Shahsavari, R. Molecular Mechanistic Origin of Nanoscale Contact, Friction, and Scratch in Complex Particulate Systems. *ACS Appl. Mater. Interfaces* **2015**, *7*, 3362−3372.
(39) Prakash, M.; Sakhavand, N.; Shahsavari, R. H2, N2, and CH4 Gas Adsorption in Zeolitic Imidazolate Framework-95 and −100: Ab Initio Based Grand Canonical Monte Carlo Simulations. *J. Phys. Chem. C* **2013**, *117*, 24407−24416.
(40) Shahsavari, R.; Chen, L. Screw dislocations in complex, low symmetry oxides: core structures, energetics, and impact on crystal growth. *ACS Appl. Mater. Interfaces* **2015**, *7*, 2223−34.
(41) Pakdel, A.; Zhi, C.; Bando, Y.; Golberg, D. Low-Dimensional Boron Nitride Nanomaterials. *Mater. Today* **2012**, *15*, 256−265.
(42) Plimpton, S. Fast Parallel Algorithms for Short-Range Molecular Dynamics. *J. Comput. Phys.* **1995**, *117*, 1−19.
(43) Albe, K.; Möller, W. Modelling of Boron Nitride: Atomic Scale Simulations on Thin Film Growth. *Comput. Mater. Sci.* **1998**, *10*, 111−115.
(44) Sekkal, W.; Bouhafs, B.; Aourag, H.; Certier, M. Molecular-Dynamics Simulation of Structural and Thermodynamic Properties of Boron Nitride. *J. Phys.: Condens. Matter* **1998**, *10*, 4975−4984.
(45) Won Ha, M.; Ho Jung, H. Molecular-Dynamics Simulation of Structure and Thermal Behaviour of Boron Nitride Nanotubes. *Nanotechnology* **2004**, *15*, 431−434.
(46) Vaccarini, L.; Goze, C.; Henrard, L.; Hernández, E.; Bernier, P.; Rubio, A. Mechanical and Electronic Properties of Carbon and Boron−Nitride Nanotubes. *Carbon* **2000**, *38*, 1681−1690.
(47) Verma, V.; Jindal, V. K.; Dharamvir, K. Elastic Moduli of a Boron Nitride Nanotube. *Nanotechnology* **2007**, *18*, 435711.

DOI: 10.1021/acsami.5b03967
ACS Appl. Mater. Interfaces 2015, 7, 18312−18319